

---

# Cycle Consistency Driven Object Discovery

---

Aniket Didolkar<sup>1</sup>, Anirudh Goyal<sup>2</sup>, Yoshua Bengio<sup>1</sup>

## Abstract

Developing deep learning models that effectively learn object-centric representations, akin to human cognition, remains a challenging task. Existing approaches have explored slot-based methods utilizing architectural priors or auxiliary information such as depth maps or flow maps to facilitate object discovery by representing objects as fixed-size vectors, called “slots” or “object files”. However, reliance on architectural priors introduces unreliability and requires meticulous engineering to identify the correct objects. Likewise, methods relying on auxiliary information are suboptimal as such information is often unavailable for most natural scenes. To address these limitations, we propose a method that explicitly optimizes the constraint that each object in a scene should be mapped to a distinct slot. We formalize this constraint by introducing consistency objectives which are cyclic in nature. We refer to them as the *cycle-consistency* objectives. By applying these consistency objectives to various existing slot-based object-centric methods, we demonstrate significant enhancements in object-discovery performance. These improvements are consistent across both synthetic and real-world scenes, highlighting the effectiveness and generalizability of the proposed approach. Furthermore, our experiments show that the learned slots from the proposed method exhibit superior suitability for downstream reinforcement learning (RL) tasks.

## 1 Introduction

Having object-based reasoning capabilities is important for solving many real-world problems. The world around us is complex, diverse, and full of distinct objects. Human beings possess the natural ability to parse and reason about these objects in their environment. Frequently, changing or manipulating certain aspects of the world requires interacting with a single object or a combination of objects. For instance, driving a car necessitates maneuvering a single object (the car) while avoiding collisions with other objects or entities such as other cars, trees, and other obstacles. Developing object-based reasoning capabilities is therefore crucial for improving the ability of deep learning models to understand and solve problems in the real world.

Existing literature provides compelling evidence that object-centric models offer more robust representations compared to their monolithic counterparts, enabling effective generalization to out-of-distribution (OOD) scenarios and proficiently solving various visual reasoning tasks. For instance, Ke et al. (2021); Dittadi et al. (2022) demonstrates the OOD generalization capabilities of object-centric models, while Assouel et al. (2022); Yang et al. (2020); Wu et al. (2023); Goyal et al. (2020, 2021b) showcase the strong reasoning abilities of these models. Additionally, several works have highlighted the usefulness of object-centric models in visual modeling Wu et al. (2023); Goyal et al. (2021b) and reinforcement learning Goyal et al. (2019); Ke et al. (2021); Yoon et al. (2023). However, the progress in object-centric approaches has been primarily confined to synthetic tasks and toy problems, with limited exploration of these approaches in real-world scenes and tasks Seitzer et al. (2023). In this study, we aim to address this gap by demonstrating the effectiveness of the proposed approach in extracting objects in both synthetic and real-world settings.

---

<sup>01</sup> Mila, University of Montreal, <sup>2</sup> Google DeepMind  
Corresponding authors: adidolkar123@gmail.com

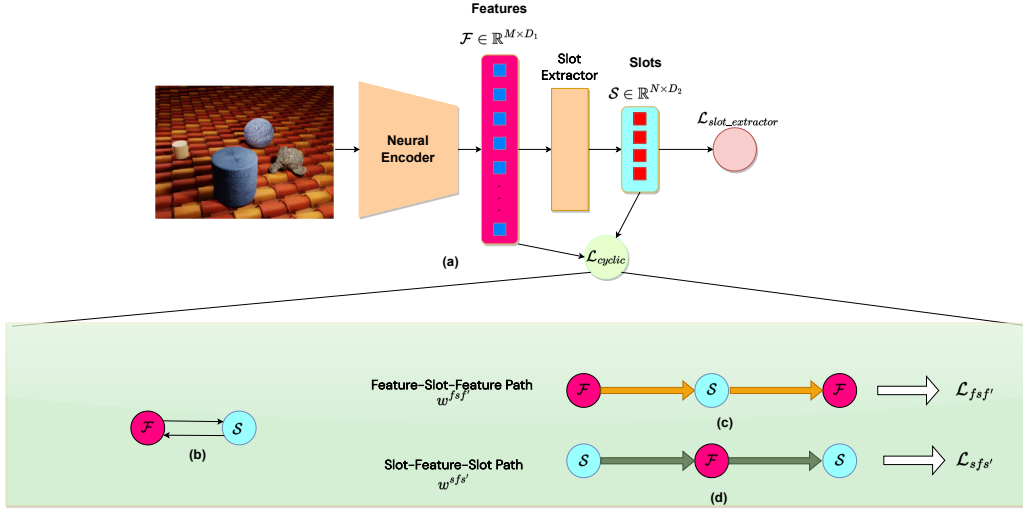


Figure 1: **Cycle Consistency Objectives.** (a) Here we show the general architecture of the model. Initially, an image is processed by an encoder, resulting in a feature set  $\mathcal{F}$ . Next, we employ a slot extractor, such as slot attention, to extract slots from the features. (b) To incorporate the cycle consistency objectives, we first construct a directed graph whose nodes constitute the slots and the features i.e. each slot and each feature is a separate node in the graph. This graph is composed of edges from slots to features and vice-versa. There is no edge between two slots or two features. We construct two types of edge paths to compute the cycle consistency objectives - (c) **FEATURE-SLOT-FEATURE Paths** - These are paths that are made up of two edges. One edge going from a particular feature  $f_i$  to a slot  $s_k$  and then another edge from slot  $s_k$  to some feature  $s_j$ . These paths are used in calculating the FEATURE-SLOT-FEATURE consistency objective which is denoted as  $\mathcal{L}_{fsf'}$ . (d) **SLOT-FEATURE-SLOT Paths** - These are also paths that are made up of two edges but in this case, the first edge originates from a particular slot  $s_i$  and goes to a feature  $f_k$  and the second edge goes from feature  $f_k$  to some slot  $s_j$ . These paths are used in calculating the SLOT-FEATURE-SLOT consistency objective which is denoted as  $\mathcal{L}_{sfs'}$ . During training, we leverage the default loss associated with the slot extractor, which is the reconstruction loss in the case of slot attention, in conjunction with both the cycle consistency objectives -  $\mathcal{L}_{final} = \mathcal{L}_{slot\_extractor} + \lambda_{fsf'} \mathcal{L}_{fsf'} + \lambda_{sfs'} \mathcal{L}_{sfs'}$

Unsupervised discovery of objects from a scene is a challenging problem, as the notion of what an object refers to may be hard to parse without any extra context. Many existing approaches Greff et al. (2017, 2019); Burgess et al. (2019); Goyal et al. (2019); Locatello et al. (2020); Goyal et al. (2020, 2021b); Ke et al. (2021); Goyal et al. (2021a); Singh et al. (2022) learn a set of slots to represent objects. Each slot is a fixed size vector. Most of these approaches use a reconstruction loss coupled with certain architectural biases that depend on visual cues to learn to segment objects into slots. There has been work that uses other auxiliary cues for supervision such as optical flow Kipf et al. (2021) and depth prediction Elsayed et al. (2022). Architectural priors may not be always reliable and hence may not scale to real-world data while relying on auxiliary information such as optical flow and motion is not feasible since many datasets and scenes do not come with this information. Instead, the proposed approach relies on explicitly enforcing coherence and consistency between the representations of the visual features (obtained from a neural encoder like convolutional or transformer-based encoder) and the learned slots. The proposed approach is simple and flexible, and it can be integrated into any slot-based object-discovery method.

To ensure coherence and consistency between the slots and features, we propose two objectives inspired by the concept of cycle consistency. Cycle consistency has been widely employed for learning representations in various visual settings Wang et al. (2013, 2014); Wilson & Snaveley (2013); Zach et al. (2010); Zhou et al. (2015a, 2016, 2015b); Hoffman et al. (2018); Zhu et al. (2017); Jabri et al. (2020). In our proposed approach, we leverage this idea to ensure *consistency* between the features and slots. Specifically, we establish two types of paths: SLOT-FEATURE-SLOT (Figure 1 (d)) and FEATURE-SLOT-FEATURE (Figure 1 (c)). In the first path, we constrain any trajectory originating from a slot to return to the same slot. In the second path, we guarantee that the trajectory

starting from a specific feature (i.e., from feature to slot and back to feature) maps to a similar feature. As we lack a ground truth measure of feature similarity, we adopt a *self-supervision* strategy and compute a feature similarity matrix which indicates how similar the two features are. We formulate these constraints as two cycle consistency objectives, denoted as  $\mathcal{L}_{sfs'}$  and  $\mathcal{L}_{fssf'}$ . Further details regarding these objectives are elaborated in Section 2.

We evaluate the proposed approach on both synthetic and real-world datasets and demonstrate its superior performance compared to other competitive baselines. We also test the model’s generalization abilities and show that it can generalize across visually similar but distinct datasets. Overall, the proposed approach provides a reliable and scalable method for unsupervised discovery of objects in visual scenes, with promising results on real-world applications.

## 2 Proposed Method

In this section, we present the details of the proposed cycle consistency objectives and the underlying intuition behind them. The proposed method is designed to operate on a set of  $N$  slots  $\mathcal{S} = \{s_0, s_1, \dots, s_N\}$  and a set of  $M$  features  $\mathcal{F} = \{f_0, f_1, \dots, f_M\}$  which can be obtained using any suitable backbone such as a convolutional encoder or a visual-transformer encoder (e.g., DINO Caron et al. (2021)). Similarly, the slots  $\mathcal{S}$  can be obtained using any suitable object discovery or slot extractor method Locatello et al. (2020); Seitzer et al. (2023) as follows:

$$\mathcal{S} = \text{slot\_extractor}(\mathcal{F}) \quad (1)$$

Figure 1 illustrates this procedure. As shown in the figure, each slot  $s_i$  is a  $D_2$ -dimensional vector and each feature  $f_i$  is a  $D_1$ -dimensional vector. Before computing the proposed cycle consistency objectives, we project the features to the same dimension as the slots using an MLP -  $\tilde{f}_i = \text{MLP}(f_i)$ . Therefore,  $\tilde{f}_i$  is a  $D_2$ -dimensional vector. Hereafter, we refer to a feature  $j$  as  $f_j$  and to use it in any computation (for example, dot product computation), we use the notation  $\tilde{f}_j$ .

### 2.1 Motivation behind the proposed idea

**Consistency between slots and features** To ensure coherence and consistency between the slots and features, we represent them as nodes in a directed graph. Each node is either a slot or a feature, and the edges represent mappings between them. The presence or absence of an edge reflects the consistency between the slot and feature representations. When the representations are fully consistent, each object in the scene is accurately represented by one slot. In this case, there exists an edge from all features corresponding to a particular object to the slot representing that object. For instance, if slot  $s_i$  represents object  $\mathcal{O}_i$ , then all features produced by the encoder that pertain to  $\mathcal{O}_i$  will have an edge leading to slot  $s_i$ . Additionally, there will also be edges in the opposite direction, from slot  $s_i$  to the features associated with  $\mathcal{O}_i$ . Importantly, there are no edges between two slots or two features. If a path exists between two features, it must pass through a slot. Therefore, the graph can be described as a bipartite graph.

Initially, the slot and feature representations lack consistency, resulting in randomly placed edges that do not adhere to the aforementioned rule. To address this, we introduce the cycle consistency objectives that ensure the representations become consistent and satisfy the rule.

**Quantifying Consistency** To quantify the consistency between a feature and a slot, we employ pairwise similarity scores based on their representations. For an edge  $s_i \rightarrow f_j$  (indicating an edge from slot  $i$  to feature  $j$ ), we compute the pairwise similarity score as follows:  $d(s_i, f_j) = s_i \cdot \tilde{f}_j$ . Subsequently, we apply the softmax operator to convert the distances into probabilities. We normalize these probabilities across all possible destination nodes for the edge. In the case mentioned above, all features serve as potential destination nodes for the edge originating from slot  $s_i$ . Specifically, the probability of an edge existing from slot  $s_i$  to feature  $f_j$  is determined by:

$$A(s_i, f_j) = \frac{\exp((s_i \cdot \tilde{f}_j)/\tau)}{\sum_{k=1}^M \exp((s_i \cdot \tilde{f}_k)/\tau)} \quad (2)$$

Similarly, the probability of the existence of an edge from feature  $f_i$  to slot  $s_j$  is given by:

$$A(f_i, s_j) = \frac{\exp((\tilde{f}_i \cdot s_j)/\tau)}{\sum_{k=1}^N \exp((\tilde{f}_i \cdot s_k)/\tau)} \quad (3)$$

For applying the cycle consistency objective, we consider two types of paths in this graph as shown in Figure 1: (1) **SLOT-FEATURE-SLOT**: Paths going from slots to features and then back to slots, i.e.,  $w^{sfs'} = s_i \rightarrow f_k \rightarrow s_j$ ; (2) **FEATURE-SLOT-FEATURE**: Paths going from features to slots and back to features, i.e.,  $w^{fsf'} = f_i \rightarrow s_k \rightarrow f_j$ .

**SLOT-FEATURE-SLOT Consistency** As previously mentioned, the objective of object discovery is to ensure that each object in the scene is represented by a distinct slot. Consequently, each slot should correspond to a unique subset of features that pertain to the object it represents. To formally achieve this, it is important that the consistency or similarity score between a slot and its corresponding subset of features (for the object that the slot represents) is high. To elaborate further, let's consider paths of the form  $w^{sfs'}$  (referred to as SLOT-FEATURE-SLOT paths). In these paths, when an edge connects a slot  $s_i$  to a feature  $f_k$ , the subsequent outgoing edge from feature  $f_k$  must return to the same slot  $s_i$ . This is because feature  $f_k$  should possess the highest similarity score with respect to slot  $s_i$  as compared to any other slots, as other slots would represent different objects. We refer to this property as **SLOT-FEATURE-SLOT Consistency**.

Initially, the SLOT-FEATURE-SLOT paths will not satisfy SLOT-FEATURE-SLOT Consistency since all edges are randomly placed. We formalize SLOT-FEATURE-SLOT consistency into an objective  $\mathcal{L}_{sfs'}$  and optimize that objective to ensure that this consistency emerges. We provide details about the objective in the next section.

**FEATURE-SLOT-FEATURE Consistency** We also apply consistency constraints to FEATURE-SLOT-FEATURE paths. In the case of full consistency, many features belonging to the same object correspond to one slot. Also, since objects are localized in space and many patches belonging to a particular object are visually similar, we can say that the features belonging to an object will develop similar representations and these features should also have a high similarity score with respect to one particular slot. Therefore, for any path  $w^{fsf'}$  which contains an edge from feature  $f_i$  to slot  $s_k$ , the outgoing edge from slot  $s_k$  can return back to multiple possible features that are close in distance to  $f_i$  and it may not return back to the same feature  $f_i$ . Therefore, here we impose the constraint that the path returns back to the same feature  $f_i$  with some probability  $p^{i \rightarrow i}$ , where  $0 < p^{i \rightarrow i} < 1$ . We calculate  $p^{i \rightarrow i}$  based on the pairwise similarity between the features. We describe the details of this in the next section. We refer to this property as **FEATURE-SLOT-FEATURE Consistency**. This consistency constraint ensures that similar features, such as those belonging to a particular object, are mapped to the same slot. Similar to SLOT-FEATURE-SLOT consistency, we formalize FEATURE-SLOT-FEATURE consistency into an objective and optimize it to achieve consistency.

Next, we state both consistency objectives succinctly and then describe how we implement these objectives.

- **SLOT-FEATURE-SLOT Consistency** - SLOT-FEATURE-SLOT consistency is achieved when a path of the form  $w^{sfs'}$  originating at a slot  $s_i$  always ends back at the same slot.
- **FEATURE-SLOT-FEATURE Consistency** - FEATURE-SLOT-FEATURE consistency is achieved when a path of the form  $w^{fsf'}$  originating at a feature  $f_i$  returns back to any of the features that are similar to  $f_i$  and may return back to the same feature  $f_i$  with some probability  $p^{i \rightarrow i}$ , where  $0 < p^{i \rightarrow i} < 1$ .

## 2.2 Implementation Details

To optimize the cycle consistency objectives, we need to compute scores for the paths  $w^{sfs'}$  and  $w^{fsf'}$  and determine the probability of a path beginning at a particular origin node ending at all possible origin nodes. For SLOT-FEATURE-SLOT consistency, we need to compute the probability of a path originating at  $s_i$  ending at  $s_k$ , where  $k \in \{1, \dots, N\}$ , for all possible slots as origin nodes.

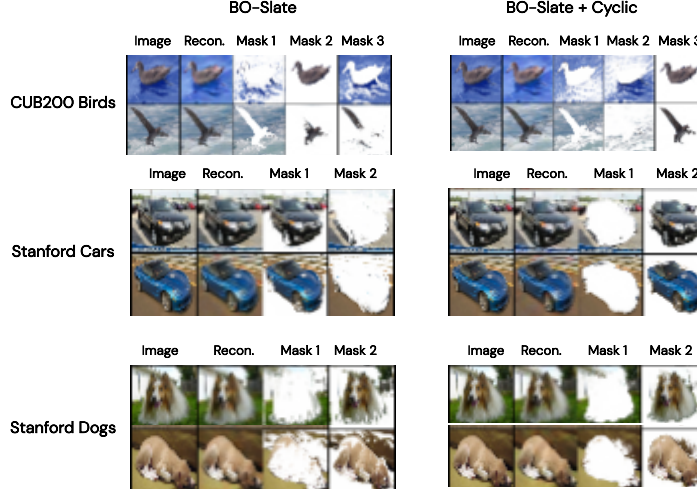


Figure 2: **Foreground Extraction Visualization.** This figure showcases the reconstruction and segmentation masks produced by the baseline model (BO-Slate) and the proposed cyclic model. Notably, we observe that the baseline model tends to mix the foreground with parts of the background, particularly for the Stanford Dogs and Stanford Cars datasets. In contrast, the use of our cyclic objectives leads to a significantly clearer separation of the foreground and background, resulting in a more accurate and refined representation of the objects of interest.

Similarly, for FEATURE-SLOT-FEATURE consistency, we need to perform the same computation while considering paths originating at the features instead of slots.

**Calculating path probabilities** For a path  $w^{sfs'}$  beginning at  $s_i$  and ending at  $s_j$ , we need to compute  $P(s_j | s_i)$ . We consider all paths beginning from  $s_i$  and ending at  $s_j$ , i.e.,  $s_i \rightarrow f_k \rightarrow s_j \quad \forall k \in \{1, \dots, M\}$ . The score for a particular path  $s_i \rightarrow f_k \rightarrow s_j$  is calculated by multiplying  $A(s_i, f_k)$  and  $A(f_k, s_j)$ . We obtain the logits for paths beginning in  $s_i$  and ending in  $s_j$  by summing this multiplication over all  $k$ , i.e.,  $\tilde{p}(s_j | s_i) = \sum_{k=1}^M A(s_i, f_k) \cdot A(f_k, s_j)$ . To convert this into a probability, we apply a softmax across all possible slots since all slots can be possible destinations for the path.

$$P(s_j | s_i) = \frac{\exp(\sum_{k=1}^M A(s_i, f_k) \cdot A(f_k, s_j) / \tau_{sfs'})}{\sum_{n=1}^N \exp(\sum_{k=1}^M A(s_i, f_k) \cdot A(f_k, s_n) / \tau_{sfs'})} \quad (4)$$

Similarly, for paths in  $w^{fsf'}$  beginning at  $f_i$  and ending at  $f_j$ , we compute  $P(f_j | f_i)$  as follows:

$$P(f_j | f_i) = \frac{\exp(\sum_{k=1}^N A(f_i, s_k) \cdot A(s_k, f_j) / \tau_{fsf'})}{\sum_{n=1}^N \exp(\sum_{k=1}^N A(f_i, s_k) \cdot A(s_k, f_n) / \tau_{fsf'})} \quad (5)$$

Note that in this case, the softmax is across all possible features since all features can be the destinations for all paths of the form  $w^{fsf'}$ .

**SLOT-FEATURE-SLOT Consistency Loss** To satisfy SLOT-FEATURE-SLOT consistency, we need to ensure that  $P(s_j | s_i)$  is 1 for all  $i = j$  and 0 otherwise. This would ensure that any path leaving a slot  $s_i$  would always cycle back to the same slot. We use a cross-entropy loss to optimize for this consistency. We refer to this as  $\mathcal{L}_{sfs'}$ :

$$\mathcal{L}_{sfs'} = -\log(P(s_j | s_i)) \quad \forall i = j \quad (6)$$

**FEATURE-SLOT-FEATURE Consistency Loss** For FEATURE-SLOT-FEATURE consistency, we want that a path originating at  $f_i$  should cycle back to any feature  $f_j$  that is close in distance to  $f_i$  and may cycle back to the same feature with some probability  $p^{i \rightarrow i}$ . Therefore, there should be some non-zero probability that a path  $w^{f_s f'}$  originating at  $f_i$  will cycle back to  $f_i$  i.e.  $0 < p^{i \rightarrow i} < 1$ . We denote the probability of a path originating at  $f_i$  and ending in  $f_j$  as  $p^{i \rightarrow j}$ . Note that,  $p^{i \rightarrow i}$  is a special case of  $p^{i \rightarrow j}$  where  $j = i$ . For FEATURE-SLOT-FEATURE consistency to be satisfied, we want  $P(f_j | f_i) = p^{i \rightarrow j} \quad \forall \quad i = j$ . The value of  $p^{i \rightarrow j}$  is computed as a function of the feature similarity scores for features  $f_i$  and  $f_j$ . We describe this procedure in detail below.

As shown in Figure 1, The visual encoder first outputs a feature matrix  $F \in \mathbb{R}^{t \times t \times D_1}$  where  $t \times t$  is the spatial dimension and  $D_1$  is the hidden dimension or output channels of the encoder. We obtain the set  $\mathcal{F}$  by flattening  $F$  across the first two dimensions, resulting in a set of size  $t^2$ . Note that,  $t^2 = M$ . Each element in  $\mathcal{F}$  is a vector of size  $D_1$ . Next, we project the features in  $\mathcal{F}$  to have the same hidden dimension as the slots using an MLP. As previously mentioned, the calculation of  $p^{i \rightarrow j}$  depends on the pairwise similarity between features. Therefore, to calculate  $p^{i \rightarrow j}$ , we first compute the dot product between  $f_i$  and  $f_j$  to obtain  $\tilde{p}^{i \rightarrow j}$ . Therefore,  $\tilde{p}^{i \rightarrow j} = \tilde{f}_i \cdot \tilde{f}_j$ . We then threshold  $\tilde{p}^{i \rightarrow j}$  using a threshold  $\theta^i$ , defined as  $\theta^i = c \cdot (\max(\mathcal{F}_i) - \min(\mathcal{F}_i)) + \min(\mathcal{F}_i)$ , where  $\mathcal{F}_i = \{\tilde{f}_i \cdot \tilde{f}_0, \tilde{f}_i \cdot \tilde{f}_1, \dots, \tilde{f}_i \cdot \tilde{f}_M\}$  is the set of similarity values between feature  $f_i$  and all other features, and  $c$  is a hyperparameter such that  $0 < c < 1$ . In our experiments, we set  $c$  to 0.8. We use the threshold  $\theta^i$  to threshold  $\tilde{p}^{i \rightarrow j}$ , so that  $\tilde{p}^{i \rightarrow j} = \tilde{f}_i \cdot \tilde{f}_j$  if  $\tilde{f}_i \cdot \tilde{f}_j > \theta^i$  else  $-\infty$ . Finally, we apply softmax to  $\mathcal{F}_i$  to obtain the probability  $p^{i \rightarrow j}$ .

$$p^{i \rightarrow j} = \frac{\exp(\tilde{p}^{i \rightarrow j})}{\sum_{k=1}^M \exp(\tilde{p}^{i \rightarrow k})} \quad (7)$$

The intuition behind using feature similarity stems from various self-supervised learning studies Grill et al. (2020); Chen et al. (2020), which aim to ensure that similar images possess similar representations. In object-centric methods, since objects are localized in space, certain features belonging to the same object will tend to close to each other in the representation space during the training process. Let us denote this set of similar features belonging to an object as  $\mathcal{K}$ , noting that  $\mathcal{K} \subset \mathcal{F}$ . As all features within  $\mathcal{K}$  share similar representations, the path probability  $p^{i \rightarrow j}$  will be high for any  $f_i \in \mathcal{K}$  and  $f_j \in \mathcal{K}$ . Moreover, to maintain FEATURE-SLOT-FEATURE consistency, these similar features should be mapped to the same slot. Therefore, we optimize the path probability of FEATURE-SLOT-FEATURE paths (i.e.,  $P(f_j | f_i)$ ) to be equal to  $p^{i \rightarrow j}$  through the utilization of a cross-entropy loss, denoted as  $\mathcal{L}_{f_s f'}$ . By employing this approach, we ensure that  $P(f_j | f_i)$  is high for features  $f_i$  and  $f_j$  that exhibit similarity, thereby facilitating their mapping to the same slot.

$$\mathcal{L}_{f_s f'} = -p^{i \rightarrow j} \log(P(f_j | f_i)) \quad \forall \quad i = j \quad (8)$$

We only compute  $\mathcal{L}_{f_s f'}$  for all  $i = j$  instead of computing it for all  $i, j$ . The reason behind this design decision is that the supervision signal, denoted as  $p^{i \rightarrow j}$ , depends on the pairwise similarity of features. It is difficult to accurately determine the pairwise feature similarity values for all combinations of  $i$  and  $j$  when training a model from scratch. As a result, we simplify the loss calculation by considering only the elements along the diagonal of the matrix, where  $i$  is equal to  $j$ . We empirically show the importance of this design choice by comparing the proposed approach against a model that calculates  $\mathcal{L}_{f_s f'}$  for all  $i, j$ . We present the results of this comparison in Appendix Table 10.

### 2.3 Training Details

The proposed method can be applied on top of any object discovery method. We incorporate our method into any slot extractor by adding the cycle consistency objectives to the original loss of the method as shown in Figure 1. For example, in slot attention Locatello et al. (2020),  $\mathcal{L}_{slot\_extractor}$  is the reconstruction loss. Thus, the final loss of the method becomes:

$$\mathcal{L}_{final} = \mathcal{L}_{recon} + \lambda_{f_s f'} \mathcal{L}_{f_s f'} + \lambda_{f_s f'} \mathcal{L}_{f_s f'} \quad (9)$$

To set the hyperparameters for our approach, we select  $\lambda_{f_s f'}$  and  $\lambda_{f_s f'}$  as 0.1 and 0.01, respectively, unless otherwise specified. We study the effect of these loss coefficients on the final performance

in Appendix Figure 5. When training models from scratch, such as with slot attention, we employ an additional Exponential Moving Average (EMA) visual encoder. This EMA encoder is used for calculating  $p^{i \rightarrow j}$  for all  $i, j \in \{1, \dots, M\}$ . This practice aligns with several self-supervised learning studies He et al. (2019); Chen & He (2020); Grill et al. (2020) and ensures that the features used in computing  $p^{i \rightarrow j}$  remain stable avoiding frequent changes caused by gradient updates in the visual encoder. To show the importance of the EMA encoder we run an experiment where we do not utilize the EMA encoder to compute  $p^{i \rightarrow j}$  and instead use the output of the online encoder to compute  $p^{i \rightarrow j}$ . We present the results of this experiment in Appendix Table 9. We find that the performance of the model drops without the EMA encoder.

We also detach the calculation of  $p^{i \rightarrow j}$  for all  $i, j \in \{1, \dots, M\}$  from the gradient computation.

In methods involving multiple iterations of object discovery, such as slot attention, we apply the cycle consistency objectives to the slots obtained from each iteration of the method, unless explicitly stated otherwise. We analyse the effect of this design choice by comparing the proposed model against a model that applies the cycle consistency objectives only to the slots from the last iteration of slot attention. We present the results of this ablation in Appendix Table 8. We find that applying the cycle consistency objectives to the slots from all iterations of slot attention is essential for achieving good performance.

We defer the discussion of related works to Appendix Section A.

### 3 Experiments

In our experiments, we aim to demonstrate the versatility of our approach by addressing the following questions:

- Can the utilization of cycle consistency objectives enhance the performance of various object discovery methods?
- Are the performance improvements consistent across both synthetic and real-world datasets?
- Does training with the proposed objective facilitate better generalization and transferability to novel scenarios?
- In addition to its benefits for object discovery, we also explore whether the learned slot representations can be useful in downstream reinforcement learning (RL) tasks, such as Atari.

**Object Discovery Approaches** We test the proposed objectives on three unsupervised object discovery approaches: (1) Slot Attention Locatello et al. (2020); (2) SLATE Singh et al. (2022); (3) Dinosaur Seitzer et al. (2023). Slot-attention uses a top-down iterative attention mechanism to discover slots from image features. The image features are obtained using a convolutional encoder. The model is trained via a reconstruction loss where the decoded images are obtained by a mixture based decoder Watters et al. (2019). SLATE uses slot-attention to discover slots but replaces the convolutional encoder in slot attention by a dVAE van den Oord et al. (2017); Ramesh et al. (2021) and the convolutional decoder by an auto-regressive transformer Ramesh et al. (2021). Dinosaur also uses slot-attention to discover slots from image features. It uses a pretrained DINO model to obtain the image features and also uses pretrained features for reconstruction based supervision. We apply the proposed objectives on top of all these approaches and demonstrate consistent performance gains. We refer to our objectives as the CYCLIC objectives.

Table 1: **Synthetic Datasets Segmentation.** In this table we compare the slot attention model augmented with the proposed CYCLIC objectives against the original slot attention model Locatello et al. (2020). As shown in the table, we observe that the proposed objectives result in performance gains across all the considered datasets. Results averaged across 3 seeds.

			ObjectsRoom		ShapeStacks		ClevrTex	
Model	$\lambda_{sfs'}$	$\lambda_{fss'}$	MSE ↓	FG-ARI ↑	MSE ↓	FG-ARI ↑	MSE ↓	FG-ARI ↑
Slot-Attention	0	0	0.0018 $\pm$ 0.0004	0.7819 $\pm$ 0.08	0.004 $\pm$ 0.0004	0.7738 $\pm$ 0.05	0.007 $\pm$ 0.001	0.6240 $\pm$ 0.223 <sup>1</sup>
+ CYCLIC	> 0	0	0.0019 $\pm$ 0.0003	0.7832 $\pm$ 0.05	0.004 $\pm$ 0.0010	0.5491 $\pm$ 0.4521	0.007 $\pm$ 0.0001	0.6640 $\pm$ 0.05
+ CYCLIC	0	> 0	0.0015 $\pm$ 0.0002	0.8120 $\pm$ 0.06	0.004 $\pm$ 0.0003	0.7755 $\pm$ 0.06	0.007 $\pm$ 0.0001	0.4974 $\pm$ 0.03
+ CYCLIC	> 0	> 0	0.0015 $\pm$ 0.0002	0.8169 $\pm$ 0.03	0.0037 $\pm$ 0.0001	0.7838 $\pm$ 0.02	0.007 $\pm$ 0.0001	0.7245 $\pm$ 0.01

**Datasets** We conduct our experiments in two domains - 1) Object Discovery and 2) Downstream RL. For object-discovery we consider both synthetic and real-world datasets. For the synthetic datasets, we use Shapestacks Groth et al. (2018), ObjectsRoom Kabra et al. (2019), ClevrTex Karazija et al. (2021), and MOVi datasets Ghorbani et al. (2020). The MOVi-C and MOVi-E variants contain realistic 3D scans of objects on HD backgrounds, with MOVi-C containing 3-10 objects per image and MOVi-E containing 11-23 objects per image. We evaluate the segmentation performance on these synthetic datasets using the Adjusted Rand Index (ARI) Hubert & Arabie (1985) and reconstruction performance using the mean-squared error (MSE). Specifically, we calculate FG-ARI for all these datasets which is same as ARI but ignores the background information. For MOVi datasets, we also report the mean best overlap (mBO) Pont-Tuset et al. (2015). mBO is calculated by assigning the predicted mask to a ground truth mask with the largest overlap and averaging the IoUs of the assigned mask pairs.

For the real-world datasets, we consider two tasks - (1) Foreground Extraction and (2) Multi-object Segmentation. For foreground extraction, we use the Stanford dogs dataset Khosla et al. (2012), Stanford cars dataset Krause et al. (2013), CUB200 Birds dataset Wah et al. (2011), and flowers dataset Nilsback & Zisserman (2006). We evaluate foreground extraction performance using mean Intersection over Union (mIoU). For multi-object segmentation, we consider the COCO Lin et al. (2014) and scannet Dai et al. (2017) datasets. We report the AP score Everingham et al. (2014), precision score and recall score for evaluating the segmentation performance of our approach on COCO and Scannet datasets.

For the downstream reinforcement learning (RL) task, we adopt the Atari environment, following the setup established by Decision Transformer Chen et al. (2021). We evaluate the effectiveness of our method by analyzing the returns obtained by the agent in each environment considered.

**Synthetic Datasets** For the synthetic tasks, we follow the setup used in Dittadi et al. (2022). We augment the slot-attention auto-encoder Locatello et al. (2020) model with the cycle consistency objectives. Slot attention uses a convolutional encoder to obtain image features  $F \in \mathbb{R}^{t \times t \times D_1}$  ( $t = 64$  for all datasets) and a mixture-based decoder for reconstruction Watters et al. (2019). Before applying the cycle consistency objectives, we downsample the features to  $\hat{F} \in \mathbb{R}^{\hat{t} \times \hat{t} \times D_1}$ , where  $\hat{t} = 16$  and then project them using an MLP to have the same dimension as the slot (i.e.  $D_2$ ). We also normalize the slots using their L2 norm before applying the cycle consistency objectives. More details regarding the architecture and hyper-parameters can be found in the Appendix Section B.

**Results.** Table 1 presents the quantitative results on all three datasets. We observe that augmenting Slot Attention with the proposed objectives leads to better factorization (as measured by FG-ARI) and superior reconstruction (measured by MSE). We also observe that while the presence of only one of the objectives does not affect the reconstruction performance significantly, having both objectives is crucial for achieving good factorization.

**ClevrTex Generalization.** The ClevrTex dataset is an extension of CLEVR that features complex scenes where both objects and backgrounds are made up of various materials, such as rocks, bricks, and tiles. To test the generalization of our approach, we use two splits from ClevrTex: (1) CAMO, which contains scenes where certain objects are camouflaged, and (2) OOD, which uses 25 new materials that were not seen during training. We train the models on the full training set of ClevrTex and transfer them to both the splits. Figure 3 presents the results, which demonstrate that the proposed method consistently outperforms the baseline on the generalization splits.

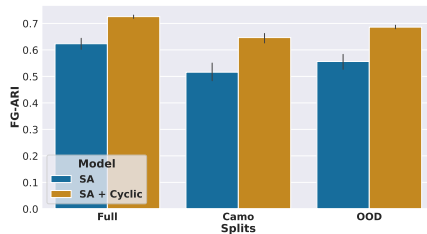


Figure 3: **ClevrTex Generalization.** Here we present transfer results on clevertex. We train the model on the *Full* split and transfer it to the *Camo* and *OOD* splits. We find that the proposed approach outperforms the baseline on both the transfer splits. Results averaged across 5 seeds.

<sup>1</sup>We took the result for SA from Karazija et al. (2021), as we were unable to reproduce the same result in a statistically consistent manner. With our implementation, we got FG-ARI score of  $0.5864_{\pm 0.01}$ . To be fair, we have reported the score from the original paper Karazija et al. (2021).



**MOVi Datasets** For the MOVi datasets, we use the setup from Seitzer et al. (2023) which presents the DINOSAUR model for object discovery. DINOSAUR applies slot attention to the features obtained from a ViT-B/8 encoder which is pretrained using the procedure presented in Caron et al. (2021). They use a reconstruction loss as the training objective to learn the slot attention parameters. The targets for the reconstruction objective are the features from the pretrained ViT model. For the proposed method, we add the cyclic objectives to the DINOSAUR model, applying them only to the slots obtained from the last iteration of slot attention. In this case, we do not use an EMA encoder, as the ViT image encoder is kept frozen through training. The results in Table 2 show that DINOSAUR augmented with cyclic objectives outperforms the base DINOSAUR model on both the datasets, demonstrating the efficacy of the proposed approach.

Table 2: **MOVi Datasets** In this table we demonstrate the improvements achieved by the cyclic objectives when added to the DINOSAUR model from Seitzer et al. (2023) based on the pretrained ViT-B/8 encoder. We can see that proposed method achieves superior performance on both the datasets.

Model	MOVi-C		MOVi-E	
	FG-ARI	mBO	FG-ARI	mBO
DINOSAUR (ViT-B/8)	68.9 $\pm$ 0.4	38.0 $\pm$ 0.2	65.1 $\pm$ 1.2	33.5 $\pm$ 0.1
+ CYCLIC	72.4 $\pm$ 2.1	40.2 $\pm$ 0.5	69.7 $\pm$ 1.6	37.2 $\pm$ 0.4

Table 3: **Unsupervised Foreground Extraction.** Here we present results for unsupervised foreground extraction on the Stanford Dogs, Stanford Cars, and CUB 200 birds dataset. We augment our cyclic objectives to the improved version of Slate Singh et al. (2022) presented in Jia et al. (2022). We can see that the performance of the Slate model improves when augmented with the proposed objectives thus showing the efficacy of our approach. Results averaged across 3 seeds.

Model	Dogs		Cars		Birds		Flowers	
	IoU $\uparrow$	Dice $\uparrow$	IoU $\uparrow$	Dice $\uparrow$	IoU $\uparrow$	Dice $\uparrow$	IoU $\uparrow$	Dice $\uparrow$
BO-Slate	0.7875 $\pm$ 0.05	0.6681 $\pm$ 0.06	0.7686 $\pm$ 0.10	0.8647 $\pm$ 0.07	0.6129 $\pm$ 0.05	0.7473 $\pm$ 0.05	0.7461 $\pm$ 0.03	0.8340 $\pm$ 0.02
+ CYCLIC	0.8456 $\pm$ 0.04	0.7462 $\pm$ 0.06	0.8447 $\pm$ 0.02	0.9145 $\pm$ 0.02	0.6497 $\pm$ 0.01	0.7797 $\pm$ 0.009	0.7745 $\pm$ 0.01	0.8525 $\pm$ 0.01

Table 4: **Real World Datasets Segmentation.** Here we present results for multi-object segmentation on real-world datasets. We augment the improved Slate model presented in Jia et al. (2022) with the proposed cyclic objectives. We can see that the proposed approach results in performance gains across all metrics on both datasets. Results averaged across 3 seeds.

Model	COCO				Scannet			
	AP@05 $\uparrow$	PQ $\uparrow$	Precision $\uparrow$	Recall $\uparrow$	AP@05 $\uparrow$	PQ $\uparrow$	Precision $\uparrow$	Recall $\uparrow$
BO-Slate	0.1664 $\pm$ 0.01	0.1748 $\pm$ 0.009	0.2549 $\pm$ 0.01	0.3113 $\pm$ 0.01	0.2467 $\pm$ 0.03	0.2355 $\pm$ 0.003	0.3403 $\pm$ 0.004	0.3874 $\pm$ 0.006
+ CYCLIC	0.1896 $\pm$ 0.009	0.1881 $\pm$ 0.008	0.2750 $\pm$ 0.01	0.3320 $\pm$ 0.01	0.2920 $\pm$ 0.01	0.2609 $\pm$ 0.01	0.3703 $\pm$ 0.01	0.4209 $\pm$ 0.01

**Real-World Datasets** For these experiments, we use the BO-SLATE model Jia et al. (2022) as our base model. BO-SLATE is an improved version of Slate Singh et al. (2022) where the main improvements come from having learnable slot initializations. We apply the cycle consistency objectives to the slots and the features as described in section 2. We defer further details to the Appendix Section C.

**Foreground Extraction** The results for this task are presented in Table 3. We observe that the proposed objectives helps the model achieve a superior performance compared to the baseline on all datasets. Additionally, in Figure 2, we visualize the reconstruction and segmentation masks from the model. We note that in certain cases, the baseline model tends to mix foreground and background information, whereas the same model augmented with the cyclic objectives is able to segregate the foreground and background information perfectly.

**Multi-Object Segmentation** The results for this task are presented in Table 4. We use the same versions of the datasets used in Jia et al. (2022). We observe that the BO-Slate model augmented with the proposed objectives outperforms the baseline on all metrics. More information about these metrics is presented in the appendix.

**Object Centric Models in Atari** One important aspect of any representation learning method is that the learned representations should be useful in downstream tasks. In this section, we explore the usefulness of object centric models in the context of atari games. Chen et al. (2021) introduced the decision transformer model which learns to play various games in the Atari suite by imitating suboptimal trajectories from a learned agent. We present more details of the decision transformer

model in Appendix Section D. In this work, we change the monolithic state representation used in decision transformer to an object-centric one.

The state representation of an observation is a  $D$ -dimensional vectors obtained by passing the atari observations through a convolutional encoder. Note that each observation is a stack of 4 frames. To obtain the corresponding object-centric version of this, we use the convolutional encoder and the slot attention module from Locatello et al. (2020) to encode each observation. Therefore, each observation is encoded into  $N$  slots instead of a single vector.

To ensure that slots learn the correct object-centric representation we augment the decision transformer loss with the slot attention loss -  $\mathcal{L} = \mathcal{L}_{DT} + \mathcal{L}_{Reconstruction}$ . In the case of cycle consistency, we also augment the cycle consistency objectives to the loss -  $\mathcal{L} = \mathcal{L}_{DT} + \mathcal{L}_{Reconstruction} + \lambda_{sfs'}\mathcal{L}_{sfs'} + \lambda_{fss'}\mathcal{L}_{fss'}$ .

The performance comparison in Table 5 reveals that the decision transformer, when augmented with object-centric representations solely obtained from slot attention (DT + SA) exhibits competitive performance across all games to the original decision transformer (DT) that utilizes monolithic representations from a CNN. However, when the object-centric decision transformer is combined with the proposed cycle consistency objectives, it surpasses the baseline decision transformer in 3 out of 4 games. This outcome not only showcases the effectiveness of object-centric representations in downstream tasks but also underscores the significance of the proposed cycle consistency objective in learning valuable object-centric representations capable of transferring effectively to downstream tasks.

#### 4 Future Work and Limitations

Significant research efforts have been dedicated to learning object-centric representations. However, the evaluation of these representations has primarily focused on unsupervised segmentation performance using metrics like ARI or IoU. Regrettably, there is a dearth of studies demonstrating the practical utility of object-centric representations across diverse downstream tasks. To address this gap, our work takes a significant stride forward by showcasing the effectiveness of our approach in the context of Atari but more work is still needed to showcase the effectiveness of these models on more complex and real-world downstream tasks. Moving forward, our objective is to shift our focus towards developing object-centric representations that prove valuable in a wide array of downstream tasks, spanning reinforcement learning to visual tasks like visual question answering and captioning. We aim to explore the efficacy of cycle consistency objectives in learning such representations and study what is lacking in building more pervasive object-centric representations.

#### 5 Acknowledgement

This research was enabled in part by compute resources provided by Mila (mila.quebec). We would like to thank Vedant Shah, Christos Kaplanis, Charles Blundell, and Ayush Chakravarthy for reviewing early versions of the manuscript.

#### References

Assouel, R., Rodriguez, P., Taslakian, P., Vazquez, D., and Bengio, Y. Object-centric compositional imagination for visual abstract reasoning. In *ICLR2022 Workshop on the Elements of Reasoning: Objects, Structure and Causality*, 2022. URL <https://openreview.net/forum?id=rCzfIruU5x5>.

Table 5: **Object-Centric Representations in Atari.** Here we present results on 4 games from the atari suite. We can see that decision transformer when augmented with object-centric representations obtained from slot attention achieve competitive performance to the baseline decision transformer which uses monolithic representations in 3 out of the 4 games. But, on combining slot attention with our proposed cycle consistency objectives, we can see that we get the best performance on 3 out of the 4 games. Results averaged across 5 seeds.

Game	DT	DT + SA	DT + SA + Cyclic
Pong	11.0 $\pm$ 5.727	7.4 $\pm$ 6.184	14.8 $\pm$ 2.482
Breakout	70.6 $\pm$ 20.539	93.4 $\pm$ 24.121	110.2 $\pm$ 11.107
Seaquest	1172.4 $\pm$ 175.779	444.0 $\pm$ 179.738	663.2 $\pm$ 111.014
Qbert	5485.2 $\pm$ 1995.256	5275.2 $\pm$ 862.894	7393.8 $\pm$ 1982.989

- Burgess, C. P., Matthey, L., Watters, N., Kabra, R., Higgins, I., Botvinick, M. M., and Lerchner, A. Monet: Unsupervised scene decomposition and representation. *CoRR*, abs/1901.11390, 2019. URL <http://arxiv.org/abs/1901.11390>.
- Caron, M., Touvron, H., Misra, I., Jégou, H., Mairal, J., Bojanowski, P., and Joulin, A. Emerging properties in self-supervised vision transformers. *CoRR*, abs/2104.14294, 2021. URL <https://arxiv.org/abs/2104.14294>.
- Chen, L., Lu, K., Rajeswaran, A., Lee, K., Grover, A., Laskin, M., Abbeel, P., Srinivas, A., and Mordatch, I. Decision transformer: Reinforcement learning via sequence modeling, 2021.
- Chen, T., Kornblith, S., Norouzi, M., and Hinton, G. E. A simple framework for contrastive learning of visual representations. *CoRR*, abs/2002.05709, 2020. URL <https://arxiv.org/abs/2002.05709>.
- Chen, X. and He, K. Exploring simple siamese representation learning. *CoRR*, abs/2011.10566, 2020. URL <https://arxiv.org/abs/2011.10566>.
- Chen, Z., Li, J., Luo, Y., Huang, Z., and Yang, Y. CANZSL: cycle-consistent adversarial networks for zero-shot learning from natural language. *CoRR*, abs/1909.09822, 2019. URL <http://arxiv.org/abs/1909.09822>.
- Choudhury, S., Laina, I., Rupprecht, C., and Vedaldi, A. Unsupervised part discovery from contrastive reconstruction. *CoRR*, abs/2111.06349, 2021. URL <https://arxiv.org/abs/2111.06349>.
- Crawford, E. and Pineau, J. Spatially invariant unsupervised object detection with convolutional neural networks. In *Proceedings of the Thirty-Third AAAI Conference on Artificial Intelligence and Thirty-First Innovative Applications of Artificial Intelligence Conference and Ninth AAAI Symposium on Educational Advances in Artificial Intelligence, AAAI'19/IAAI'19/EAAI'19*. AAAI Press, 2019. ISBN 978-1-57735-809-1. doi: 10.1609/aaai.v33i01.33013412. URL <https://doi.org/10.1609/aaai.v33i01.33013412>.
- Dai, A., Chang, A. X., Savva, M., Halber, M., Funkhouser, T., and Nießner, M. Scannet: Richly-annotated 3d reconstructions of indoor scenes. In *Proc. Computer Vision and Pattern Recognition (CVPR), IEEE*, 2017.
- Dittadi, A., Papa, S., De Vita, M., Schölkopf, B., Winther, O., and Locatello, F. Generalization and robustness implications in object-centric learning. In *International Conference on Machine Learning*, 2022.
- Dwibedi, D., Aytar, Y., Tompson, J., Sermanet, P., and Zisserman, A. Temporal cycle-consistency learning. *CoRR*, abs/1904.07846, 2019. URL <http://arxiv.org/abs/1904.07846>.
- Elsayed, G. F., Mahendran, A., van Steenkiste, S., Greff, K., Mozer, M. C., and Kipf, T. SAVi++: Towards end-to-end object-centric learning from real-world videos. In Oh, A. H., Agarwal, A., Belgrave, D., and Cho, K. (eds.), *Advances in Neural Information Processing Systems*, 2022. URL <https://openreview.net/forum?id=fT9W531LxNS>.
- Engelcke, M., Kosiorek, A. R., Jones, O. P., and Posner, I. Genesis: Generative scene inference and sampling with object-centric latent representations. *arXiv preprint arXiv:1907.13052*, 2019.
- Eslami, S. M. A., Heess, N., Weber, T., Tassa, Y., Szepesvari, D., kavukcuoglu, k., and Hinton, G. E. Attend, infer, repeat: Fast scene understanding with generative models. In Lee, D., Sugiyama, M., Luxburg, U., Guyon, I., and Garnett, R. (eds.), *Advances in Neural Information Processing Systems*, volume 29. Curran Associates, Inc., 2016. URL [https://proceedings.neurips.cc/paper\\_files/paper/2016/file/52947e0ade57a09e4a1386d08f17b656-Paper.pdf](https://proceedings.neurips.cc/paper_files/paper/2016/file/52947e0ade57a09e4a1386d08f17b656-Paper.pdf).
- Everingham, M., Eslami, S. M. A., Gool, L. V., Williams, C. K. I., Winn, J. M., and Zisserman, A. The pascal visual object classes challenge: A retrospective. *International Journal of Computer Vision*, 111:98–136, 2014.
- Ghorbani, S., Mahdavian, K., Thaler, A., Körding, K. P., Cook, D. J., Blohm, G., and Troje, N. F. Movi: A large multipurpose motion and video dataset. *CoRR*, abs/2003.01888, 2020. URL <https://arxiv.org/abs/2003.01888>.

- Goyal, A., Lamb, A., Hoffmann, J., Sodhani, S., Levine, S., Bengio, Y., and Schölkopf, B. Recurrent independent mechanisms. *arXiv preprint arXiv:1909.10893*, 2019.
- Goyal, A., Lamb, A., Gampa, P., Beaudoin, P., Levine, S., Blundell, C., Bengio, Y., and Mozer, M. Object files and schemata: Factorizing declarative and procedural knowledge in dynamical systems. *arXiv preprint arXiv:2006.16225*, 2020.
- Goyal, A., Didolkar, A., Lamb, A., Badola, K., Ke, N. R., Rahaman, N., Binas, J., Blundell, C., Mozer, M., and Bengio, Y. Coordination among neural modules through a shared global workspace. *arXiv preprint arXiv:2103.01197*, 2021a.
- Goyal, A., Didolkar, A. R., Ke, N. R., Blundell, C., Beaudoin, P., Heess, N., Mozer, M. C., and Bengio, Y. Neural production systems. In Beygelzimer, A., Dauphin, Y., Liang, P., and Vaughan, J. W. (eds.), *Advances in Neural Information Processing Systems*, 2021b. URL <https://openreview.net/forum?id=xQGYquca0gB>.
- Greff, K., van Steenkiste, S., and Schmidhuber, J. Neural expectation maximization. *CoRR*, abs/1708.03498, 2017. URL <http://arxiv.org/abs/1708.03498>.
- Greff, K., Kaufman, R. L., Kabra, R., Watters, N., Burgess, C., Zoran, D., Matthey, L., Botvinick, M. M., and Lerchner, A. Multi-object representation learning with iterative variational inference. *CoRR*, abs/1903.00450, 2019. URL <http://arxiv.org/abs/1903.00450>.
- Grill, J.-B., Strub, F., Altché, F., Tallec, C., Richemond, P., Buchatskaya, E., Doersch, C., Avila Pires, B., Guo, Z., Gheshlaghi Azar, M., Piot, B., kavukcuoglu, k., Munos, R., and Valko, M. Bootstrap your own latent - a new approach to self-supervised learning. In Larochelle, H., Ranzato, M., Hadsell, R., Balcan, M., and Lin, H. (eds.), *Advances in Neural Information Processing Systems*, volume 33, pp. 21271–21284. Curran Associates, Inc., 2020. URL [https://proceedings.neurips.cc/paper\\_files/paper/2020/file/f3ada80d5c4ee70142b17b8192b2958e-Paper.pdf](https://proceedings.neurips.cc/paper_files/paper/2020/file/f3ada80d5c4ee70142b17b8192b2958e-Paper.pdf).
- Groth, O., Fuchs, F. B., Posner, I., and Vedaldi, A. Shapestacks: Learning vision-based physical intuition for generalised object stacking. *ArXiv*, abs/1804.08018, 2018.
- Hadji, I., Derpanis, K. G., and Jepson, A. D. Representation learning via global temporal alignment and cycle-consistency. In *Proceedings of the IEEE/CVF Conference on Computer Vision and Pattern Recognition (CVPR)*, pp. 11068–11077, June 2021.
- He, K., Fan, H., Wu, Y., Xie, S., and Girshick, R. B. Momentum contrast for unsupervised visual representation learning. *CoRR*, abs/1911.05722, 2019. URL <http://arxiv.org/abs/1911.05722>.
- H’enaff, O. J., Koppula, S., Shelhamer, E., Zoran, D., Jaegle, A., Zisserman, A., Carreira, J., and Arandjelović, R. Object discovery and representation networks. In *European Conference on Computer Vision*, 2022.
- Hoffman, J., Tzeng, E., Park, T., Zhu, J.-Y., Isola, P., Saenko, K., Efros, A., and Darrell, T. CyCADA: Cycle-consistent adversarial domain adaptation. In Dy, J. and Krause, A. (eds.), *Proceedings of the 35th International Conference on Machine Learning*, volume 80 of *Proceedings of Machine Learning Research*, pp. 1989–1998. PMLR, 10–15 Jul 2018. URL <https://proceedings.mlr.press/v80/hoffman18a.html>.
- Hu, X., Wang, R., Zhou, D., and Xiong, Y. Neural topic modeling with cycle-consistent adversarial training. *CoRR*, abs/2009.13971, 2020. URL <https://arxiv.org/abs/2009.13971>.
- Huang, Y., Zhu, W., Xiong, D., Zhang, Y., Hu, C., and Xu, F. Cycle-consistent adversarial autoencoders for unsupervised text style transfer. *CoRR*, abs/2010.00735, 2020. URL <https://arxiv.org/abs/2010.00735>.
- Hubert, L. J. and Arabie, P. Comparing partitions. *Journal of Classification*, 2:193–218, 1985.
- Jabri, A., Owens, A., and Efros, A. A. Space-time correspondence as a contrastive random walk. *CoRR*, abs/2006.14613, 2020. URL <https://arxiv.org/abs/2006.14613>.

- Jia, B., Liu, Y., and Huang, S. Improving object-centric learning with query optimization, 2022. URL <https://arxiv.org/abs/2210.08990>.
- Kabra, R., Burgess, C., Matthey, L., Kaufman, R. L., Greff, K., Reynolds, M., and Lerchner, A. Multi-object datasets. <https://github.com/deepmind/multi-object-datasets/>, 2019.
- Karazija, L., Laina, I., and Rupprecht, C. Clevrtex: A texture-rich benchmark for unsupervised multi-object segmentation. *ArXiv*, abs/2111.10265, 2021.
- Ke, N. R., Didolkar, A., Mittal, S., Goyal, A., Lajoie, G., Bauer, S., Rezende, D., Bengio, Y., Mozer, M., and Pal, C. Systematic evaluation of causal discovery in visual model based reinforcement learning. *arXiv preprint arXiv:2107.00848*, 2021.
- Khosla, A., Jayadevaprakash, N., Yao, B., and Fei-Fei, L. Novel dataset for fine-grained image categorization : Stanford dogs. 2012.
- Kipf, T., Elsayed, G. F., Mahendran, A., Stone, A., Sabour, S., Heigold, G., Jonschkowski, R., Dosovitskiy, A., and Greff, K. Conditional object-centric learning from video. *CoRR*, abs/2111.12594, 2021. URL <https://arxiv.org/abs/2111.12594>.
- Krause, J., Stark, M., Deng, J., and Fei-Fei, L. 3d object representations for fine-grained categorization. In *4th International IEEE Workshop on 3D Representation and Recognition (3DRR-13)*, Sydney, Australia, 2013.
- Lai, Z. and Xie, W. Self-supervised learning for video correspondence flow. *CoRR*, abs/1905.00875, 2019. URL <http://arxiv.org/abs/1905.00875>.
- Lee, S. and Lee, M. Type-dependent prompt CycleQAG : Cycle consistency for multi-hop question generation. In *Proceedings of the 29th International Conference on Computational Linguistics*, pp. 6301–6314, Gyeongju, Republic of Korea, October 2022. International Committee on Computational Linguistics. URL <https://aclanthology.org/2022.coling-1.549>.
- Li, X., Liu, S., Mello, S. D., Wang, X., Kautz, J., and Yang, M. Joint-task self-supervised learning for temporal correspondence. *CoRR*, abs/1909.11895, 2019. URL <http://arxiv.org/abs/1909.11895>.
- Lin, T.-Y., Maire, M., Belongie, S. J., Hays, J., Perona, P., Ramanan, D., Dollár, P., and Zitnick, C. L. Microsoft coco: Common objects in context. In *European Conference on Computer Vision*, 2014.
- Lin, Z., Wu, Y., Peri, S. V., Sun, W., Singh, G., Deng, F., Jiang, J., and Ahn, S. SPACE: unsupervised object-oriented scene representation via spatial attention and decomposition. *CoRR*, abs/2001.02407, 2020. URL <http://arxiv.org/abs/2001.02407>.
- Locatello, F., Weissenborn, D., Unterthiner, T., Mahendran, A., Heigold, G., Uszkoreit, J., Dosovitskiy, A., and Kipf, T. Object-centric learning with slot attention. In Larochelle, H., Ranzato, M., Hadsell, R., Balcan, M., and Lin, H. (eds.), *Advances in Neural Information Processing Systems*, volume 33, pp. 11525–11538. Curran Associates, Inc., 2020. URL <https://proceedings.neurips.cc/paper/2020/file/8511df98c02ab60aea1b2356c013bc0f-Paper.pdf>.
- Nilsback, M.-E. and Zisserman, A. A visual vocabulary for flower classification. In *IEEE Conference on Computer Vision and Pattern Recognition*, volume 2, pp. 1447–1454, 2006.
- Pont-Tuset, J., Arbelaez, P., Barron, J. T., Marqués, F., and Malik, J. Multiscale combinatorial grouping for image segmentation and object proposal generation. *CoRR*, abs/1503.00848, 2015. URL <http://arxiv.org/abs/1503.00848>.
- Ramesh, A., Pavlov, M., Goh, G., Gray, S., Voss, C., Radford, A., Chen, M., and Sutskever, I. Zero-shot text-to-image generation. *CoRR*, abs/2102.12092, 2021. URL <https://arxiv.org/abs/2102.12092>.
- Seitzer, M., Horn, M., Zadaianchuk, A., Zietlow, D., Xiao, T., Simon-Gabriel, C.-J., He, T., Zhang, Z., Schölkopf, B., Brox, T., and Locatello, F. Bridging the gap to real-world object-centric learning. In *The Eleventh International Conference on Learning Representations*, 2023. URL [https://openreview.net/forum?id=b9tUk-f\\_aG](https://openreview.net/forum?id=b9tUk-f_aG).

- Shah, M., Chen, X., Rohrbach, M., and Parikh, D. Cycle-consistency for robust visual question answering. *CoRR*, abs/1902.05660, 2019. URL <http://arxiv.org/abs/1902.05660>.
- Singh, G., Deng, F., and Ahn, S. Illiterate DALL-e learns to compose. In *International Conference on Learning Representations*, 2022. URL <https://openreview.net/forum?id=h00YV0We3oh>.
- van den Oord, A., Vinyals, O., and kavukcuoglu, k. Neural discrete representation learning. In Guyon, I., Luxburg, U. V., Bengio, S., Wallach, H., Fergus, R., Vishwanathan, S., and Garnett, R. (eds.), *Advances in Neural Information Processing Systems*, volume 30. Curran Associates, Inc., 2017. URL <https://proceedings.neurips.cc/paper/2017/file/7a98af17e63a0ac09ce2e96d03992fbc-Paper.pdf>.
- Wah, C., Branson, S., Welinder, P., Perona, P., and Belongie, S. Caltech-ucsd birds 200. Technical Report CNS-TR-2011-001, California Institute of Technology, 2011.
- Wang, F., Huang, Q., and Guibas, L. J. Image co-segmentation via consistent functional maps. In *2013 IEEE International Conference on Computer Vision*, pp. 849–856, 2013. doi: 10.1109/ICCV.2013.110.
- Wang, F., Huang, Q., Ovsjanikov, M., and Guibas, L. J. Unsupervised multi-class joint image segmentation. In *2014 IEEE Conference on Computer Vision and Pattern Recognition*, pp. 3142–3149, 2014. doi: 10.1109/CVPR.2014.402.
- Wang, H., Liang, W., Shen, J., Gool, L. V., and Wang, W. Counterfactual cycle-consistent learning for instruction following and generation in vision-language navigation. *2022 IEEE/CVF Conference on Computer Vision and Pattern Recognition (CVPR)*, pp. 15450–15460, 2022a.
- Wang, N., Song, Y., Ma, C., Zhou, W., Liu, W., and Li, H. Unsupervised deep tracking. *CoRR*, abs/1904.01828, 2019. URL <http://arxiv.org/abs/1904.01828>.
- Wang, Y., Shen, X., Hu, S. X., Yuan, Y., Crowley, J. L., and Vafreydaz, D. Self-supervised transformers for unsupervised object discovery using normalized cut. *2022 IEEE/CVF Conference on Computer Vision and Pattern Recognition (CVPR)*, pp. 14523–14533, 2022b.
- Watters, N., Matthey, L., Burgess, C. P., and Lerchner, A. Spatial broadcast decoder: A simple architecture for learning disentangled representations in vaes. *CoRR*, abs/1901.07017, 2019. URL <http://arxiv.org/abs/1901.07017>.
- Wilson, K. and Snavely, N. Network principles for sfm: Disambiguating repeated structures with local context. In *2013 IEEE International Conference on Computer Vision*, pp. 513–520, 2013. doi: 10.1109/ICCV.2013.69.
- Wu, Z., Dvornik, N., Greff, K., Kipf, T., and Garg, A. Slotformer: Unsupervised visual dynamics simulation with object-centric models. In *The Eleventh International Conference on Learning Representations*, 2023. URL <https://openreview.net/forum?id=TFbwV6I0VLg>.
- Yang, J., Mao, J., Wu, J., Parikh, D., Cox, D., Tenenbaum, J. B., and Gan, C. Object-centric diagnosis of visual reasoning. *ArXiv*, abs/2012.11587, 2020.
- Yoon, J., Wu, Y.-F., Bae, H., and Ahn, S. An investigation into pre-training object-centric representations for reinforcement learning, 2023.
- Zach, C., Klopschitz, M., and Pollefeys, M. Disambiguating visual relations using loop constraints. In *2010 IEEE Computer Society Conference on Computer Vision and Pattern Recognition*, pp. 1426–1433, 2010. doi: 10.1109/CVPR.2010.5539801.
- Zhou, T., Lee, Y. J., Yu, S. X., and Efros, A. A. Flowweb: Joint image set alignment by weaving consistent, pixel-wise correspondences. In *2015 IEEE Conference on Computer Vision and Pattern Recognition (CVPR)*, pp. 1191–1200, 2015a. doi: 10.1109/CVPR.2015.7298723.
- Zhou, T., Krähenbühl, P., Aubry, M., Huang, Q., and Efros, A. A. Learning dense correspondence via 3d-guided cycle consistency. *CoRR*, abs/1604.05383, 2016. URL <http://arxiv.org/abs/1604.05383>.

Zhou, X., Zhu, M., and Daniilidis, K. Multi-image matching via fast alternating minimization. In *2015 IEEE International Conference on Computer Vision (ICCV)*, pp. 4032–4040, 2015b. doi: 10.1109/ICCV.2015.459.

Zhu, J., Park, T., Isola, P., and Efros, A. A. Unpaired image-to-image translation using cycle-consistent adversarial networks. *CoRR*, abs/1703.10593, 2017. URL <http://arxiv.org/abs/1703.10593>.

Zoran, D., Kabra, R., Lerchner, A., and Rezende, D. J. Parts: Unsupervised segmentation with slots, attention and independence maximization. In *2021 IEEE/CVF International Conference on Computer Vision (ICCV)*, pp. 10419–10427, 2021. doi: 10.1109/ICCV48922.2021.01027.

## Appendix

### A Related Work

**Unsupervised Object Discovery** Our work addresses the problem of object discovery in visual scenes. While this challenge has been tackled using supervised, semi-supervised, and unsupervised methods, our approach falls into the category of unsupervised object discovery techniques Greff et al. (2017, 2019); Burgess et al. (2019); Eslami et al. (2016); Lin et al. (2020); Goyal et al. (2020); Crawford & Pineau (2019); Zoran et al. (2021); Locatello et al. (2020); Ke et al. (2021); Engelcke et al. (2019); Goyal et al. (2019, 2021b). These techniques rely on a set of vectors, known as *slots*, to represent objects, and use various architectural priors and objectives to group image features into slots that correspond to distinct objects. However, a limitation of these methods is that they have only been evaluated on synthetic datasets. To overcome this limitation, Singh et al. (2022) introduced SLATE, which uses a transformer-based decoder to decode slots into images, as opposed to a mixture-based decoder Watters et al. (2019) used by other prior methods. Moreover, Jia et al. (2022) extended SLATE to work with more complex real-world datasets, such as COCO Lin et al. (2014), Scannet Dai et al. (2017), and CUB200 Birds Wah et al. (2011). Some methods use contrastive learning to learn good representations for object discovery H’enaiff et al. (2022); Choudhury et al. (2021). For instance, Choudhury et al. (2021) use contrastive objectives to ensure that features belonging to the same parts have similar representations and that the assignment of pixels to slots is consistent across different views of the image. On the other hand, H’enaiff et al. (2022) use two networks to discover objects. One network produces object proposals, and the other produces better representations using a contrastive objective. The contrastive objective is applied to object-level features using proposals produced by the first network. Most of these approaches jointly learn the image features and slots end-to-end. Recently, some works Seitzer et al. (2023); Choudhury et al. (2021); Wang et al. (2022b) have clustered features obtained from a pretrained model into slots. While many of these works have shown promising results for object discovery, they do not explicitly enforce consistency or correspondence between the image features and the slots. Most existing approaches rely on architectural priors or various objectives (e.g., contrastive objectives Choudhury et al. (2021); H’enaiff et al. (2022)) to recover objects. However, these approaches do not explicitly encode the information that each slot must represent a distinct object. In contrast, our proposed cycle consistency objectives explicitly optimize for this, i.e., the objectives enforce each slot to represent a distinct object. Furthermore, our proposed objectives do not require multiple views of the scene, as in Choudhury et al. (2021), or multiple networks, as in H’enaiff et al. (2022). The proposed objectives are simple and can be easily integrated into any slot-based object discovery method.

**Cycle Consistency** Cycle consistency is a concept in deep learning that enables the learning of a consistent mapping between two domains in cases where 1-to-1 data is not available. It relies on the property of transitivity to enforce structure in representations, and has been successfully used for learning good representations in images, videos, and language. Numerous studies Wang et al. (2013, 2014); Wilson & Snavely (2013); Zach et al. (2010); Zhou et al. (2015a, 2016, 2015b); Hoffman et al. (2018); Zhu et al. (2017) have employed cycle consistency in image-based tasks such as co-segmentation, domain transfer, and image matching. In these works, cycle consistency is typically used as an objective function that ensures the consistency of the mapping between the source and target domains, and the inverse mapping from the target domain back to the source domain. For example, in Zhu et al. (2017), the source and target domains are images from distinct styles.

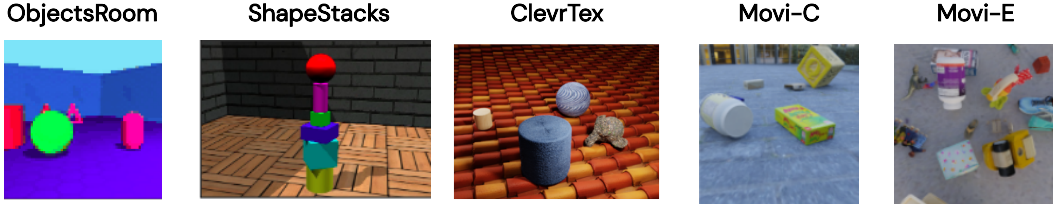


Figure 4: Here we show an example image from each synthetic dataset that we consider.

	ObjectsRoom				ShapeStacks				ClevrTex			
Layer	Channels	Kernel Size	Padding	Stride	Channels	Kernel Size	Padding	Stride	Channels	Kernel Size	Padding	Stride
Convolutional Encoder												
Conv	32	5	2	1	32	5	2	1	64	5	2	1
Conv	32	5	2	1	32	5	2	1	64	5	2	1
Conv	32	5	2	1	32	5	2	1	64	5	2	1
Conv	32	5	2	1	32	5	2	1	64	5	2	1
Convolutional Decoder												
Conv. Trans	32	5	2	1	32	5	2	1	64	5	2	2
Conv. Trans	32	5	2	1	32	5	2	1	64	5	2	2
Conv. Trans	32	5	2	1	32	5	2	1	64	5	2	2
Conv. Trans	4	5	1	1	32	5	2	1	4	5	2	1

Table 6: Detailed architecture for the encoder and decoder used by the slot attention model used in the synthetic dataset experiments. Note that we use relu activations after every layer except the last layer.

Cycle consistency has also been utilized as a self-supervised representation learning technique in videos. Various studies Dwibedi et al. (2019); Wang et al. (2019); Li et al. (2019); Lai & Xie (2019); Jabri et al. (2020); Hadji et al. (2021) have used the cycle consistency objective to enforce temporal consistency in videos, ensuring that there is a path forward from frame  $i$  to frame  $k$ , and the path backward from frame  $k$  lands back on frame  $i$ . Furthermore, cycle consistency has also been applied in different language settings where paired training data is not available (Huang et al. (2020); Hu et al. (2020); Lee & Lee (2022)), and in multimodal visual-language settings Chen et al. (2019); Wang et al. (2022a); Shah et al. (2019). Our work differs from previous works in that it is the first to apply the cycle consistency objective for object discovery. Additionally, the domains used in this study are different latent spaces: the feature space and the slot space while previous studies have primarily focused on language, images, or videos as domains.

## B Synthetic Dataset Experiments

We consider the Shapestacks Groth et al. (2018), ObjectsRoomKabra et al. (2019), ClevrTex Karazija et al. (2021), and MOVi datasets Ghorbani et al. (2020). Figure 4 shows an example image from each dataset.

**Slot Attention Implementation Details** For ObjectsRoom, ShapeStacks, and ClevrTex, we use slot attention as our base model. Table 6 shows the detailed architecture of the convolutional encoder and decoder used by the slot attention model. Table 7 indicates values of various hyperparameters used in these experiments. For each experiment, we use 1 RTX8000 GPU.

**Effect of applying the objectives on all iterations of slot attention** One implementation detail for the proposed method is that we apply the cycle consistency objectives to slots from all iterations of slot attention. We run an ablation on ClevrTex where we test the performance of the approach when we apply the proposed cycle consistency objectives only to the last iteration of slot attention. We present results in Table 8. We can see that the performance drops significantly when the cycle consistency objectives are only applied to the last iteration thus showing the importance of applying the objectives on all iterations.

**Effect of EMA Encoder** Another implementational detail of our approach is that we use an EMA encoder to compute the feature similarity probabilities  $p^{i \rightarrow i}$ . We examine the importance of using an EMA encoder by comparing the performance of the proposed approach on the shapestacks datasets with and without it. We present the results of this comparison in Table 9. We can see that the



	ObjectsRoom	ShapeStacks	ClevrTex
Num. Slots	7	7	11
Num. Iter	3	3	3
Slot size	64	64	64
MLP size	128	128	128
Batch Size	64	64	64
Optimizer	Adam	Adam	Adam
LR	0.0004	0.0004	0.0004
Total steps	500k	500k	500k
Warmup Steps	10k	10k	5k
Decay Steps	100k	100k	50k
$\lambda_{sfs'}$	0.1	0.1	0.1
$\lambda_{fssf'}$	0.01	0.01	0.01
$\tau$	0.1	0.1	0.1
$\tau_{sfs'}$	1	1	1
$\tau_{fssf'}$	0.01	0.01	0.01
$\theta_i$	0.8	0.8	0.8
Downsampled feature size	$16 \times 16$	$16 \times 16$	$32 \times 32$
EMA Decay rate	0.995	0.995	0.995

Table 7: This table indicates all the values for various hyperparameters used in the synthetic dataset experiments.

Table 8: In this table we present results of an ablation where instead of applying the cycle consistency objectives to the slots from all the iterations of slot attention, we apply it to only the slots from the last iteration. We can see that the performance drops significantly when applied only to the last iteration thus underscoring the importance of applying the objectives to each iteration of slot attention. We performed this ablation on the ClevrTex dataset. Results averaged across 5 seeds.

Model	FG-ARI
SA + Cyclic (last iteration only)	0.5453 $\pm$ 0.06
SA + Cyclic (all iterations)	0.7245 $\pm$ 0.01

performance of the model with the EMA encoder is much better than the performance without it thus showing the importance of the EMA encoder.

**Effect of Loss coefficients** We study the effect of the loss coefficients ( $\lambda_{sfs'}$  and  $\lambda_{fssf'}$ ) in Figure 5. We can see that for the variation in  $\lambda_{sfs'}$  (Figure 5 (a)), the performance degrades rapidly for higher values. We conjecture that the reason behind this is that SLOT-FEATURE-SLOT consistency can be trivially satisfied if all features are mapped to one slot. Therefore, having a high  $\lambda_{sfs'}$  may bias the model towards the trivial solution hence hurting performance. From Figure 5(b), we can see that the performance variation is much more stable in the case where we vary the value of  $\lambda_{fssf'}$ . This shows that the model is fairly agnostic to the value of  $\lambda_{fssf'}$ .

**Ablation on  $\mathcal{L}_{fssf'}$  application** In our case, we calculate  $\mathcal{L}_{fssf'}$  as follows:  $\mathcal{L}_{fssf'} = -p^{i \rightarrow j} \log(P(f_j | f_i)) \quad \forall \quad i = j$ . Therefore, instead of computing the loss for all pairs of  $i$  and  $j$ , we only compute it for the cases where  $i$  is equal to  $j$ . This design choice is made because the supervision signal,  $p^{i \rightarrow j}$ , is a function of the pairwise feature similarity values. Obtaining accurate pairwise feature similarity values for all  $i, j$  in a model trained from scratch is challenging. Hence,

Table 9: In this table we compare the performance of the proposed approach with and without the EMA encoder. The EMA encoder is used to compute the feature similarity probabilities. We can see that the performance of the model without the EMA encoder is much worse than with it thus showing the importance of the EMA encoder. We run this experiment on the shapestacks dataset.

Model	FG-ARI
SA + Cyclic (No EMA Encoder)	0.7028 $\pm$ 0.03
SA + Cyclic (EMA Encoder)	0.7838 $\pm$ 0.02

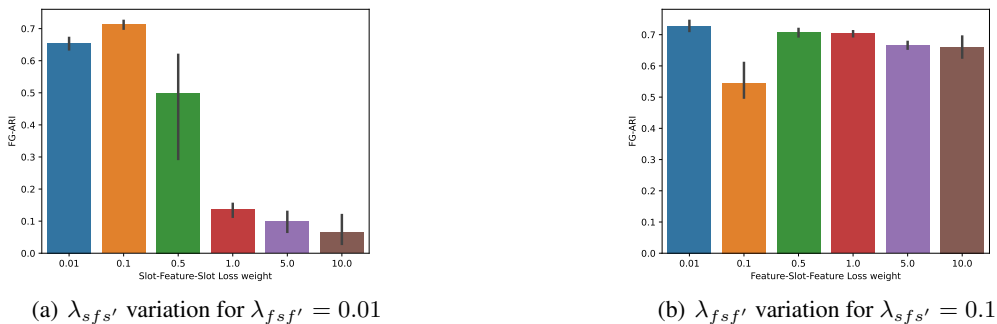


Figure 5: Here we vary the loss coefficients for the cycle consistency objectives and examine its effects on the final performance for the ClevrTex dataset. (a) In this we vary the SLOT-FEATURE-SLOT weight ( $\lambda_{sfsf'}$ ) and keep the FEATURE-SLOT-FEATURE weight ( $\lambda_{fsf'}$ ) fixed to 0.01. We can see that the model reaches peak performance for  $\lambda_{sfsf'} = 0.1$  and the performance degrades rapidly for higher values. (b) In this we vary  $\lambda_{fsf'}$  and keep  $\lambda_{sfsf'}$  fixed to 0.1. We can see that the performance is much more stable here as compared to varying  $\lambda_{sfsf'}$ .

	ObjectsRoom	ShapeStacks	ClevrTex
Model	FG-ARI	FG-ARI	FG-ARI
SA + Cyclic ( $\mathcal{L}_{fsf'} \forall i, j$ )	0.7341 $\pm$ 0.07	0.7161 $\pm$ 0.01	0.6349 $\pm$ 0.11
SA + Cyclic ( $\mathcal{L}_{fsf'} \forall i = j$ )	0.8169 $\pm$ 0.03	0.7838 $\pm$ 0.02	0.7245 $\pm$ 0.01

Table 10: Here we compare the performance of the model where  $\mathcal{L}_{fsf'}$  is computed for all  $i, j$  to the model which computes  $\mathcal{L}_{fsf'}$  for all  $i = j$ . We can see that the latter performs better than former thus showing the importance of computing the  $\mathcal{L}_{fsf'}$  only for  $i = j$ . We perform this ablation on the ObjectsRoom, ShapeStacks, and ClevrTex datasets.

we limit the loss calculation to only the diagonal elements of the matrix, where  $i = j$ . To assess the significance of this design choice, we compare the performance of the proposed model with a model that computes  $\mathcal{L}_{fsf'}$  for all  $i, j$ . The results of this study are presented in Table 10. Notably, computing  $\mathcal{L}_{fsf'}$  solely for  $i = j$  yields considerably better performance compared to computing it for all  $i, j$ .

**Dinosaur Implementation Details** We use DINOSAUR Seitzer et al. (2023) as the base model to which we augment the cycle consistency objectives for our experiments on the MOVIE and MOVIC datasets. We use a pretrained ViT-B/8 model pretrained using the approach presented in DINO Caron et al. (2021). We use 10 slots for experiments on the MOVIC dataset and 23 slots for experiments on the MOVIE dataset. For both datasets, we use 3 slot attention iterations. In this case, we apply the cycle consistency objectives on the slots obtained from the last iteration of slot attention. We set  $\lambda_{sfsf'}$  to 5 and  $\lambda_{fsf'}$  to 1. We use Adam optimizer with a learning rate of 4e-4. We run each experiment on 1 RTX8000 GPU.

## C Real World Dataset Experiments

For these experiments, we use the BO-Slate Jia et al. (2022) as the base model to which we augment the cycle consistency objectives. The values of all hyperparameters used for these experiments are shown in Table 11.

**Unsupervised Foreground Extraction** For foreground extraction, we use the Stanford dogs dataset Khosla et al. (2012), Stanford cars dataset Krause et al. (2013), CUB200 Birds dataset Wah et al. (2011), and flowers dataset Nilsback & Zisserman (2006). We evaluate the performance using the IoU (Intersection over union) and the Dice metrics. IoU is calculated by dividing the overlapping area between the ground-truth and predicted masks by the union area of the ground-truth and predicted

Training	batch size warmup steps learning rate max steps Input image size	64 10000 1e-4 250k 96 × 96
dVAE	vocabulary size Gumbel-Softmax annealing range Gumbel-Softmax annealing steps lr-dVAE (no warmup)	1024 1.0 to 0.1 30000 3e-4
Transformer Decoder	layer heads dropout hidden dimension	4 4 0.1 256
Slot Attention Module	slot dimension iterations $\sigma$ annealing steps	256 3 30000
Cycle Consistency Objective	$\lambda_{sfs'}$ $\lambda_{fsf'}$ $\tau$ $\tau_{sfs'}$ $\tau_{fsf'}$ $\theta_i$ EMA Decay rate Downsampled Feature size	10 1 0.1 1 0.01 0.8 0.900 24 × 24

Table 11: This table shows various hyperparameters used in the real-world dataset experiments where we use BO-Slate as the base model.

masks. Dice is calculated as twice the area of overlap between the ground-truth and predicted mask divide by the combined number of pixels between the ground-truth and predicted masks.

We follow the hyperparameters mentioned in Table 11. We use 2 slots for all foreground extraction experiments except for Birds for which we use 3 slots. To downsample the features obtained from the encoder for computing the cycle consistency objectives, we use a 2 layered convolutional network in which each layer has kernel size 4, stride 2, and padding 1. We use a relu activation between the two layers. We run each experiment on 1 RTX8000 GPU.

**Multi-Object Segmentation** For multi-object segmentation, we use the coco Lin et al. (2014) and scannet Dai et al. (2017) datasets. We use the following metrics to evaluate performance -

- AP@05: AP is a metric used in object detection to measure the accuracy and relevance of detection results based on precision and recall values.
- Panoptic Quality (PQ): PQ is a comprehensive metric for evaluating object segmentation that combines segmentation quality and instance-level recognition performance into a single score.
- Precision score: Precision measures the proportion of correctly predicted foreground pixels among all the pixels predicted as foreground, indicating the accuracy of the segmentation results.
- Recall Score: Recall measures the proportion of correctly predicted foreground pixels among all the ground truth foreground pixels, indicating the completeness or coverage of the segmentation results.

We use the same hyperparameters as presented in Table 11. For calculating the cycle consistency objective, we downsample the features output by the encoder using a similar convolutional network as used in the Foreground Extraction task.

	Channels	Layer	Kernel Size	Padding	Stride	output padding
Convolutional Encoder	Conv.	64	5	2	1	
	Conv.	64	5	2	1	
	Conv.	64	5	2	1	
	Conv	64	5	2	1	
Convolutional Decoder	Conv Trans.	64	7	0	2	0
	Conv Trans.	32	3	1	2	1
	Conv Trans.	5 (4 for frames + 1 for mask)	3	1	2	1

Table 12: Architecture of the encoder and decoder used in the slot attention module for the decision transformer model.

Hyperparameter	Value
slot dimension	256
iterations	3
$\lambda_{sfs'}$	0.1
$\lambda_{fsf'}$	0.01
$\tau$	0.1
$\tau_{sfs'}$	1
$\tau_{fsf'}$	0.01
$\theta_i$	0.8
EMA Decay rate	0.995
Downsampled Feature size	$21 \times 21$

Table 13: Here we present the values for the various hyperparameters used in the slot attention module for the decision transformer experiments.

## D Object Centric Models in Atari

We follow the exact setup from decision transformer Chen et al. (2021) for this experiment. Decision Transformer models the offline RL problem as a conditional sequence modelling task. This is done by feeding into the model the states, actions, and the return-to-go  $\hat{R}_c = \sum_{c'=c}^C r_{c'}$ , where  $c$  denotes the timesteps. This results in the following trajectory representation:  $\tau = (\hat{R}_1, s_1, a_1, \hat{R}_2, s_2, a_2, \hat{R}_3, s_3, a_3, \dots)$ , where  $a_c$  denotes the actions and  $s_c$  denotes the states. At test time, the start state  $s_1$  and desired return  $\hat{R}_1$  is fed into the model and it autoregressively generates the rest of the trajectory.

The original state representations  $s_i$  are  $D$ -dimensional vectors obtained by passing the atari observations through a convolutional encoder. Note that each observation is a stack of 4 frames. To obtain the corresponding object-centric version of this, we use the convolutional encoder and the slot attention module from Locatello et al. (2020) to encode each observation. Therefore, each observation is encoded into  $N$  slots resulting in a decision transformer trajectory -  $\tau = (\hat{R}_1, \{s_1^1, s_1^2 \dots, s_1^N\}, a_1, \hat{R}_2, \{s_2^1, s_2^2 \dots, s_2^N\}, a_2, \hat{R}_3, \{s_3^1, s_3^2 \dots, s_3^N\}, a_3, \dots)$ .

As mentioned in the main text, we augment the action-prediction loss from decision transformer with the reconstruction loss from slot attention and the proposed cycle consistency objectives.

We use a 6-layered transformer and 8 attention heads with an embedding size 128. We use a batch size of 64. We use a context length of 50 for Pong and a context length of 30 for Seaquest, Breakout, and Qbert. We keep all other hyperparameters same as mentioned in Chen et al. (2021). For the slot attention implementation, we define the architecture of the encoder and decoder in Table 12. The values of the other hyperparameters related to the slot attention module and the cycle consistency objectives are presented in Table 13. The input image size for the atari experiments is  $84 \times 84$ . We downsample the features to size  $21 \times 21$  to compute the cycle consistency objectives. We use a 2-layered convolutional network for this downsampling where each layer has kernel size 4, stride 2, and padding 1.